

Inorganic–Organic Hybrid Composites Containing MQ (II–VI) Slabs: A New Class of Nanostructures with Strong Quantum Confinement and Periodic Arrangement

Xiaoying Huang, Harry R. Heulings IV, Vina Le, and Jing Li*

Department of Chemistry, Rutgers University, Camden, New Jersey 08102

Received May 22, 2001. Revised Manuscript Received June 7, 2001

A new class of nanostructures has been prepared and characterized. These nanocomposite hybrid materials are composed of two-dimensional MQ (II–VI) slabs and organic bifunctional molecules that act as links as well as spacers. The most intriguing properties of these nanostructures are that they exhibit strong quantum confinement effect while possessing a perfectly periodic arrangement. The crystal structures of [MnSe(en)_{0.5}] (**1**; en = ethylenediamine), [MnSe(pda)_{0.5}] (**2**; pda = propanediamine), [ZnSe(en)_{0.5}] (**3**), and [ZnSe(pda)_{0.5}] (**4**) have been analyzed by single crystal and powder X-ray diffraction methods. Compounds **1** and **3** are isostructural and crystallize in orthorhombic crystal system, space group *Pbca* (No. 61), *Z* = 4. Crystal data for **1**: *a* = 6.711(1), *b* = 6.614(1), *c* = 17.720(4) Å. For **3**: *a* = 6.6326(7), *b* = 6.4630(6), *c* = 17.3540(16) Å. Compounds **2** and **4** are isostructural and crystallize in orthorhombic crystal system, space group *Cmc2₁* (No. 36), *Z* = 4. Crystal data for **2**: *a* = 20.384(4), *b* = 6.719(1), *c* = 6.565(1) Å. For **4**: *a* = 19.9731(18), *b* = 6.6268(7), *c* = 6.4394(6) Å. The optical absorption experiments show that both **3** and **4** generate a very large blue shift in the absorption edge (1.4–1.5 eV), and both compounds are thermally stable up to 250 °C.

Introduction

Semiconductor nanostructures with uniform arrangement, for example, periodic arrays of quantum dots (QDs), are necessary to achieve a sharp line width and strong intensity for practical applications in optoelectronic devices.¹ Quantum dots grown by colloidal methods are highly attractive because of their small sizes and strong capability in modifying electronic and optical properties of the semiconductor bulk materials.^{2a} For example, the InP dots with size ranging 2–6 nm in diameter can shift the optical gaps by as much as 1 eV.^{2b} The great challenge, however, is to generate uniformly sized dots and to organize them into periodic arrays.³ On the other hand, self-assembled strain dots can have quite uniform structures, but their ability in changing optical properties is severely limited.⁴ These difficulties can substantially limit their uses.

Recently, we have initiated a research program to explore a new class of quantum-confined nanostructures. These compounds are capable of modifying certain electronic and optical properties of II–VI systems on the same large scale as colloidal dots, and at the same time they possess uniform structures.⁵ The structures of these hybrid materials are constructed in such a way that they contain II–VI fragments as a source of semiconductor functionality and organic spacers as links or nodes to the inorganic motifs in an ordered fashion. The approach is unconventional and unique in that the electron-confining layers are formed by breaking a periodic, three-dimensional II–VI semiconductor host lattice into segments and reorganizing them using organic spacers via stable and desirable coordinate or covalent bonds in an ordered manner. Thus, a uniform structure is naturally obtained (Scheme 1). Furthermore, since the quantum confinement effect (QCE) induced in these hybrid composite materials is a result of inherent structural properties, the restriction on size and size distribution can be lifted, and particles with tunable electronic and optical properties resembling quantum dots but with physical dimensions on the micrometer, rather than nanometer scale, may be generated. It is worth noting that many synthetic methods produce particles typically in the length scale of micrometers (μm). In contrast, the properties of the nanoparticles grown by colloidal methods depend strongly on the particle size, and since they are formed via uncorrelated nucleus cores, it is difficult to generate dots

* To whom correspondence should be addressed.

(1) Gourley, P. L. *Sci. Am.* **1998** (Mar), 58. Levi, R. G. *Phys. Today* **1996** (May), 22. Klein, D. L.; Roth, Lim A. K.; Alivisatos, A. P.; McEuen, P. *Nature* **1997**, *389*, 699.

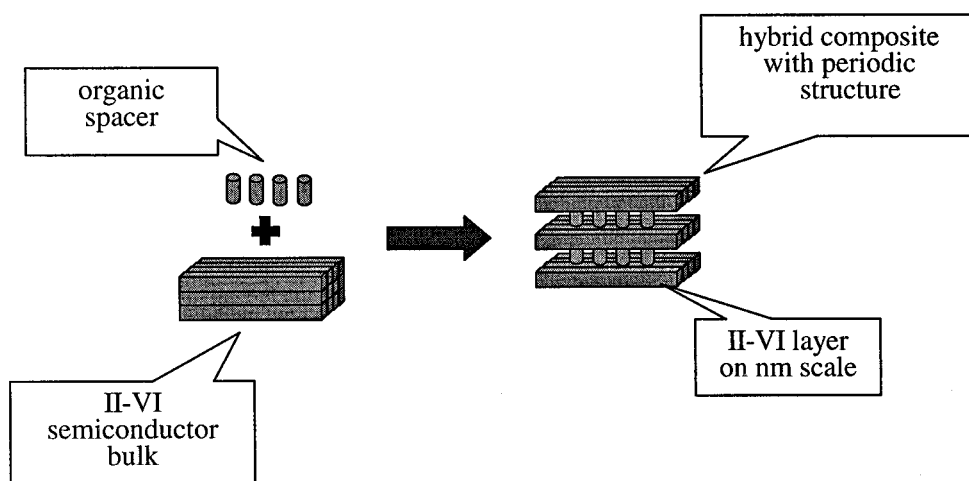
(2) (a) Norris, D. J.; Bawendi, M. G. *J. Am. Chem. Soc.* **1993**, *115*, 8706. Alivisatos, A. P. *Science* **1996**, *271*, 933. Empedocles, S. A.; Norris, D. J.; Bawendi, M. G. *Phys. Rev. Lett.* **1996**, *77*, 3873. Alivisatos, A. P. *MRS Bull.* **1998**, *23*, 17. (b) Micic, O. I.; Cheong, H. M.; Fu, H.; Zunger, Sprague J. R.; Mascarenhas, A.; Nozik, A. *J. Phys. Chem. B* **1997**, *101*, 4901.

(3) Nozik, A. J.; Micic, O. I. *MRS Bull.* **1998**, *23*, 24.

(4) Marzin, J. Y.; Gerard, J. M.; Izrael, A.; Barrier, D.; Bastard, G. *Phys. Rev. Lett.* **1994**, *73*, 716. Grundmann, M.; Bimberg, D. *Phys. Rev. B* **1997**, *55*, 9740. Kim, J.; Wang, L. W.; Zunger, A. *Phys. Rev. B* **1997**, *56*, R15541. Heitz, R.; Ramachandran, T. R.; Kalburge, A.; Xie, Q.; Mukhametzhanov, I.; Chen, P.; Madhukar, A. *Phys. Rev. Lett.* **1997**, *78*, 4071.

(5) Huang, X.-Y.; Li, J.; Fu, H. *J. Am. Chem. Soc.* **2000**, *122*, 8789.

Scheme 1



with narrow size distribution and ordered structure. The hybrid materials considered here can be regarded as a novel “superlattice” alternating with the II–VI layer and the organic layer. However, unlike the conventional semiconductor superlattices where the band offset introduces only a weak confinement, the insulating organic layer imposes a strong confinement on the semiconductor layer and will, therefore, give rise to a significant modification in the bulk properties. In addition, these materials will possess the same features and properties as other organic–inorganic hybrid composites that are important for the miniaturization of electronic and optical devices: for example, superior electronic and optical properties as well as rigidity and stability due to the inorganic component; and high processability, flexibility, lightweight, and structural diversity due to the organic component. In this article, we describe the synthesis and structure characterization of four members of this family and report their optical and thermal properties.

Experimental Section

Materials and Instruments. MnCl_2 (97%, Alfa Aesar), ZnCl_2 (98%, Aldrich), Se (99.5%, Strem), ethylenediamine (en, 99%, anhydrous, Aldrich), and 1,3-propanediamine (pda, 98%, anhydrous, Alfa Aesar). All chemicals were used as received without further purification. Powder X-ray diffraction (PXRD) of samples was performed on a Rigaku D/M-2200T automated diffraction system (Ultima⁺). The structure analyses were carried out using JADE (Windows) and GSAS software packages. The calculated PXRD patterns were generated from the single-crystal data. Optical diffuse reflectance spectra were measured at room temperature with a Shimadzu UV-3101PC double beam, double monochromated spectrophotometer. Thermogravimetric analyses (TGA) were performed on a computer controlled TA Instrument TGA-2050 system.

Synthesis of $[\text{MnSe}(\text{en})_{0.5}]$ (1). Single crystals of **1** were obtained by solvothermal reactions containing 0.063 g of MnCl_2 (0.50 mmol) and 0.020 g of Se (0.25 mmol). The starting materials were weighed and mixed and then transferred to a thick-walled Pyrex tube, and 0.4 mL of ethylenediamine was added. After the liquid was condensed by liquid nitrogen, the tube was sealed with a torch under vacuum ($\sim 10^{-3}$ Torr). The sample was then heated at 160 °C for 7 days. After being cooled to room temperature, the mixture was washed with 30 and 80% ethanol followed by drying in anhydrous ethyl ether. Orange-reddish platelike crystals (0.040 g, 96.3% yield based on Se) of **1** were obtained.

Synthesis of $[\text{MnSe}(\text{pda})_{0.5}]$ (2). Reactions of MnCl_2 (0.031 g, 0.25 mmol), Se (0.020 g, 0.25 mmol), and 1,3-propanediamine (0.4 mL) in a mole ratio of 1:1:19 at 125 °C for 12 days in thick-wall Pyrex tubes afforded orange platelike crystals of **2** (0.031 g, 71.6% yield based on Se). The same experimental procedure used for the synthesis of **1** was applied here.

Synthesis of $[\text{ZnSe}(\text{en})_{0.5}]$ (3). Compound **3** was obtained from the reactions of ZnCl_2 (0.273 g, 2 mmol), Se (0.079 g, 1 mmol), and en (5 mL) in a mole ratio of 2:1:75 in a 23 mL acid digestion bomb at 140 °C for 8 days. The product was washed by 30% ethanol and water followed by drying in anhydrous ethyl ether. The tan powder of **3** (0.155 g, 88.9% based on Se) was isolated.

Synthesis of $[\text{ZnSe}(\text{pda})_{0.5}]$ (4). Compound **4** was prepared from the reactions of ZnCl_2 (0.273 g, 2 mmol), Se (0.079 g, 1 mmol), and pda (6 mL) in a mole ratio of 2:1:75 in a 23 mL acid digestion bomb at 140 °C for 8 days. The product was washed by 30% ethanol and water followed by drying in anhydrous ethyl ether. The tan powder of **4** (0.130 g, 71.7% based on Se) was isolated.

Structure Analysis. Intensity data of compounds **1** and **2** were collected at room temperature (293 ± 1 K) on an automated Enraf-Nonius CAD4 diffractometer with graphite monochromated Mo $K\alpha$ radiation. Single crystals with dimensions of $0.18 \times 0.15 \times 0.02$ mm (**1**) and $0.20 \times 0.10 \times 0.02$ mm (**2**) were mounted on a glass fiber and placed onto the goniometer head in air. Lattice parameters were obtained from least-squares analysis of 25 computer-centered reflections with $6.81^\circ \leq \theta \leq 11.35^\circ$ (**1**) and $6.61^\circ \leq \theta \leq 13.11^\circ$ (**2**). Data collection were monitored by three standards every 2 h. No decay was observed except the statistic fluctuation in the range of $\pm 1.5\%$ (**1**) and $\pm 5.5\%$ (**2**). Raw intensities were corrected for Lorentz and polarization effects, and for absorption by empirical method based on ψ -scan data. Direct phase determination and subsequent difference Fourier map synthesis yielded the positions of Mn, Se, N, and C atoms, all of which were subjected to anisotropic refinement. Hydrogen atoms were located from difference Fourier maps, and their thermal parameters were set equal to $1.2 U_{\text{eq}}$ of the parent nonhydrogen atoms. An extinction correction was applied and refined to 0.0010(**2**) and 0.0147(**9**) (**2**). The final full-matrix, least-squares refinement on F^2 converged with $R1 = 0.0278$ and $wR2 = 0.0655$ for 634 observed reflections ($I > 2\sigma(I)$) and 38 variables (**1**) and $R1 = 0.0367$ and $wR2 = 0.0886$ for 1007 observed reflections ($I > 2\sigma(I)$) and 44 variables (**2**). The largest shift/esd in the final cycle of refinement was 0.000. The largest peaks in the final difference Fourier maps were $0.595 \text{ e}/\text{\AA}^3$ (**1**) and $1.162 \text{ e}/\text{\AA}^3$ (**2**). The absolute structural parameter for **2** is $-0.04(4)$. Details of crystal parameters, data collection, and structure refinements are given in Table 1. All computations were performed using the SHELX97 program package,⁶ and crystal structure drawings were produced with SCHAKAL 97.⁷

Table 1. Crystallographic Data for 1 and 2

	1	2
empirical formula	C ₂ H ₈ N ₂ Se ₂ Mn ₂	C ₃ H ₁₀ N ₂ Se ₂ Mn ₂
fw	327.90	341.93
space group	<i>Pbca</i> (No.61)	<i>Cmc2₁</i> (No.36)
<i>a</i> (Å)	6.711(1)	20.384(4)
<i>b</i> (Å)	6.614(1)	6.719(1)
<i>c</i> (Å)	17.720(4)	6.565(1)
<i>V</i> (Å ³)	786.5(2)	899.1(3)
Z	4	4
<i>T</i> (K)	293(2)	293(2)
λ (Å)	0.710 73	0.710 73
ρ_{calc} (g cm ⁻³)	2.769	2.526
μ (mm ⁻¹)	12.372	10.829
<i>P</i> α (<i>I</i> > 2 σ (<i>I</i>))	0.0278	0.0367
<i>R_w</i> ^b	0.0655	0.0886

^a $R = \sum ||F_o| - |F_c|| / \sum |F_o|$. ^b $R_w = [\sum w(|F_o|^2 - |F_c|^2)|^2 / \sum w(F_o^2)]^{1/2}$.
Weighting: $w = 1/\sigma^2[F_o^2 + (0.032P)^2]$ **1**, where $P = (F_o^2 + 2F_c^2)/3$;
 $w = 1/\sigma^2[F_o^2 + (0.032P)^2 + 2.0P]$ **2**.

Table 2. Atomic Coordinates and Equivalent Isotropic Temperature Factors (Å²) for 1 and 2

atoms	x	y	z	U _{eq}
Compound 1				
Mn	0.6050(1)	0.1546(1)	0.2981(1)	0.022(1)
Se	0.9566(1)	0.0280(1)	0.3242(1)	0.021(1)
N	0.4571(6)	0.0120(6)	0.3938(3)	0.024(1)
C	0.5404(7)	0.0623(8)	0.4678(3)	0.027(1)
H(1)	0.3279	0.0408	0.3980	0.029
H(2)	0.4803	0.1184	0.3827	0.029
H(3)	0.5152	0.1986	0.4703	0.033
H(4)	0.6836	0.0603	0.4640	0.033
Compound 2				
Mn	0.2083(1)	0.1502(2)	0.4982(2)	0.021(1)
Se	0.1849(1)	0.2024(1)	0.1209(2)	0.020(1)
N	0.1233(3)	0.3006(8)	0.6323(13)	0.023(1)
C(1)	0.0607(4)	0.2318(13)	0.5525(13)	0.033(2)
C(2)	0	0.3173(16)	0.6516(18)	0.029(2)
H(1)	0.1263	0.2908	0.7849	0.027
H(2)	0.1188	0.4519	0.6345	0.027
H(3)	0.0592	0.0900	0.5698	0.039
H(4)	0.0603	0.2604	0.4008	0.039
H(5)	0	0.3023	0.8302	0.035
H(6)	0	0.4658	0.6608	0.035

^a U_{eq} is defined as one-third of the trace of the orthogonalized **U** tensor.

The final atomic coordinates and the equivalent isotropic displacement parameters for **1** and **2** are listed in Table 2.

The powder diffraction analyses of compounds **3** and **4** were performed on a Rigaku D/M-2200T automated diffraction system (Ultima⁺). Measurements were made in a 2θ range of 8–100° for **3** and 6–100° for **4**, respectively. The data were collected at room temperature with a step size of 0.01° and a counting time of 10 s/step at the operating power of 46 kV/(40 mA). The powder patterns were indexed by TREOR^{8a} method using program PowderX.^{8b} The resulting unit cell parameters as well as the atomic parameters, space groups of the isostructural compounds **1** and **2** were input as initial values for Rietveld profile refinement in GSAS.⁹ After the initial refinement of the scale, background, and unit cell parameters, the profile parameters LX, LY, trns, asym, shft, GP, stec, ptec, sfec, were refined one by one. The preferred orientation corrections were done by applying spherical harmonics func-

(6) Sheldrick, G. M. *SHELX-97: Program For Structure Refinement*; University of Göttingen: Göttingen, Germany, 1997.

(7) Keller, E. *SCHAKAL 97: A Computer Program for Graphical Representation of Molecular and Crystallographic Models*; University of Freiburg: Freiburg, Germany, 1997.

(8) (a) Werner, P. E.; Eriksson, L.; Westdahl, M. *J. Appl. Crystallogr.* **1985**, *18*, 367. (b) Dong, C. *J. Appl. Crystallogr.* **1999**, *32*, 838.

(9) Larson, A. C.; Von Dreele, R. B. *GSAS, Generalized Structure Analysis System*; Los Alamos National Laboratory: Los Alamos, NM, 1998.

Table 3. Crystallographic Data for 3 and 4

	3	4
empirical formula	C ₂ H ₈ N ₂ Se ₂ Zn ₂	C ₃ H ₁₀ N ₂ Se ₂ Zn ₂
fw	348.76	362.79
space group	<i>Pbca</i> (No.61)	<i>Cmc2₁</i> (No.36)
<i>a</i> (Å)	6.6298(9)	19.9731(18)
<i>b</i> (Å)	6.4608(9)	6.6268(7)
<i>c</i> (Å)	17.350(2)	6.44394(6)
<i>V</i> (Å ³)	744.0(2)	852.31(14)
Z	4	4
<i>T</i> (K)	293(2)	293(2)
λ (Å)	1.5405, 1.5443	1.5405, 1.5443
ρ_{calc} (g cm ⁻³)	3.117	2.825
μ (mm ⁻¹)	16.15	14.08
pattern range (2θ deg)	8–100	6–100
step size (2θ deg)	0.01	0.01
step scan time (s)	10	10
no. of contributing reflns ($K\alpha_1 + K\alpha_2$)	813	505
no of struct params	68	62
<i>R_{wp}</i>	0.1344	0.1614
<i>R_p</i>	0.0877	0.1124
<i>R</i> (<i>F</i> ²)	0.0514	0.0569

Table 4. Atomic Coordinates for 3 and 4

atoms	x	y	z
Compound 3			
Zn	0.6021(4)	0.1510(5)	0.30049(12)
Se	0.9451(4)	0.0228(4)	0.31957(12)
N	0.4324(24)	0.0269(32)	0.3959(7)
C	0.5381(30)	0.0785(29)	0.4723(8)
Compound 4			
Zn	0.20561(18)	0.1563(6)	0.4927(13)
Se	0.18904(13)	0.1922(4)	0.1199(12)
N	0.1218(8)	0.3186(30)	0.641(4)
C(1)	0.0539(11)	0.2306(29)	0.541(4)
C(2)	0	0.330(5)	0.655(4)

tion. Finally atomic positions were refined. Hydrogen atoms were not included. No corrections for absorption effects were made. The details of the Rietveld refinements are described in Table 3. Positional parameters are given in Table 4.

Thermal Analysis. Thermogravimetric (TG) analyses of the title compounds were performed on a computer controlled TA Instrument 2050TGA analyzer. Single phased powder samples of **3** (10.308 mg) and **4** (10.340 mg) were loaded into platinum pans and heated with a ramp rate of 10 °C/min from room temperature to 415 °C.

Diffuse Reflectance Measurements. Optical diffuse reflectance spectra were collected at room temperature with a Shimadzu UV-3101PC double beam, double monochromator spectrophotometer. Data were measured in the wavelength range of 250–2000 nm. BaSO₄ powder was used as a standard (100% reflectance). A similar procedure as previously described¹⁰ was used to collect and convert the data using the Kubelka–Munk function.¹¹ The scattering coefficient (*S*) was treated as a constant since the average particle size of the samples used in the measurements was significantly larger than 5 mm.

Results and Discussion

Structure Description. All four compounds were synthesized solvothermally using ethylenediamine (**1**, **3**) and 1,3-propanediamine (**2**, **4**) as solvents. The crystal structure of **1** is a three-dimensional network containing monolayer of ²[MnSe] slabs that are interconnected by bridging en molecules. Figure 1a illustrates a view of **1**

(10) Li, J.; Chen, Z.; Wang, X.-X.; Proserpio, D. M. *J. Alloys Compd.* **1997**, *262–263*, 28.

(11) Wendlandt, W. WM.; Hecht, H. G. *Reflectance Spectroscopy*; Interscience, A Division of John Wiley & Sons: New York, 1966.

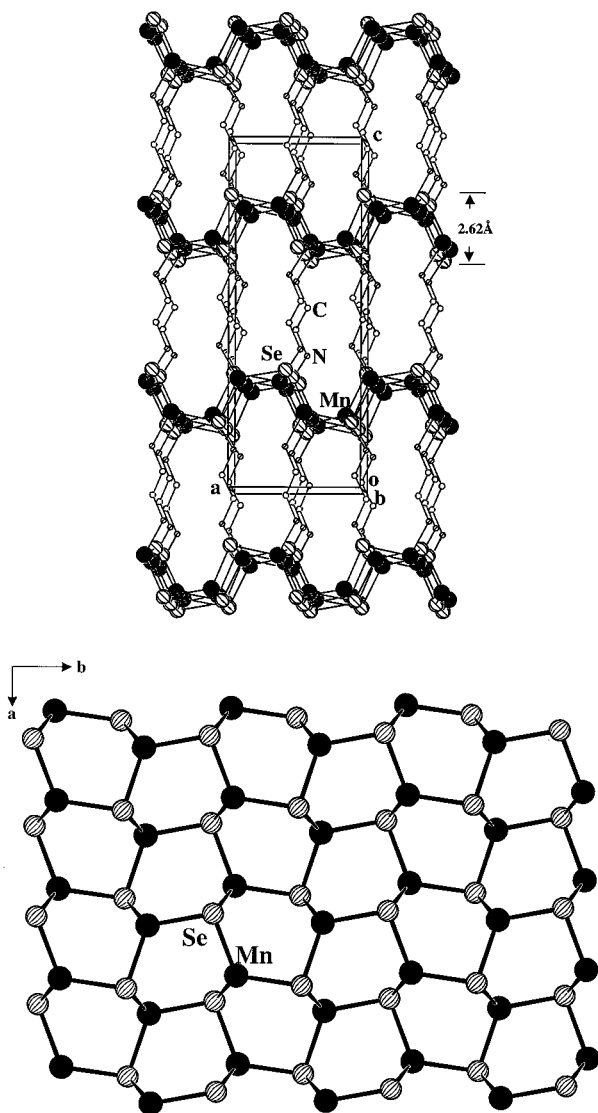


Figure 1. (a, top) View of structure **1** shown along the *b*-axis with the unit cell outlined. The large solid circles are Mn, shaded circles Se, and small open and singly shaded circles C and N, respectively. The thickness of the 2D [MnSe] monolayer is indicated in the figure (~ 2.62 Å). (b, bottom) 2D [MnSe] slab projected along the *c*-axis.

along the *b*-axis. The ${}^2_{\infty}$ [MnSe] slab is a puckered 6^3 (honeycomb) net formed by alternating three-coordinated Mn and Se (Figure 1b). It can be regarded as a "slice" cut from the parent zinc blende or wurtzite type structure of MnSe.¹² The interconnection between any two adjacent slabs are made by en molecules bridged to two metal atoms from the two slabs. Structure **2** is very similar to **1**. As depicted in Figure 2, the inorganic slabs are almost identical in the two structures. The only difference is in the organic pillars, with ethylenediamine in **1** and 1,3-propanediamine in **2**. Compounds **3** and **4** are isostructural to **1** and **2**, respectively. Their room temperature powder X-ray diffraction patterns are shown in Figure 3, compared to the simulated patterns from single-crystal data of **1** and **2**. The ${}^2_{\infty}$ [MSe] (*M* = Mn, Zn) slabs have a thickness that falls well below the

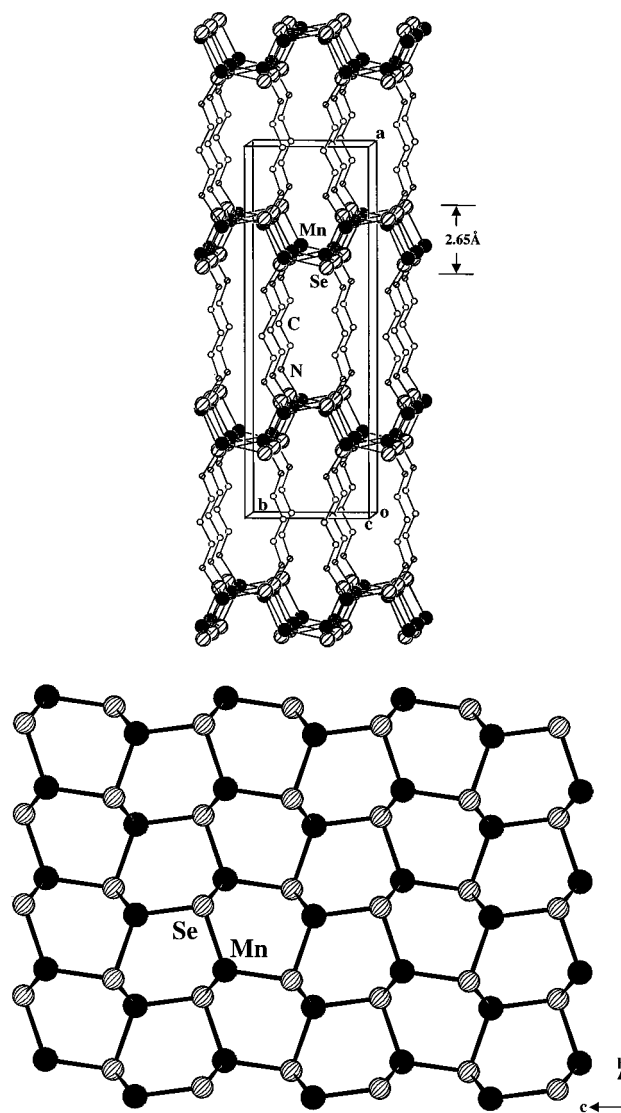


Figure 2. (a, top) View of **2** along the *c*-axis. The thickness of the 2D [MnSe] monolayer is indicated in the figure (~ 2.65 Å). The same labeling scheme as in Figure 1 is used here. (b, bottom) 2D [MnSe] slab projected along the *b*-axis.

nanometer regime (e.g. 0.262 and 0.265 nm for **1** and **2**, respectively). In fact, this thickness is at a single atomic monolayer, the smallest possible length scale that can be achieved by a quantum-confined II–VI system. These highly correlated, yet well-separated nanometer-sized semiconductor fragments thus represent an unprecedented type of nanostructures, and a very strong QCE is anticipated, provided the metal 3d bands are not highly localized.¹³

Optical Properties. The optical absorption spectra of **3** and **4** were measured by diffuse reflectance experiments,^{10–11} and the results are plotted in Figure 4, along with that of ZnSe (Stilleite).¹⁴ The absorption edges for **3** and **4** are found to be of 4.0 and 3.9 eV, respectively. Compared to the measured value of 2.5 eV for ZnSe (Stilleite), it clearly indicates a very large blue shift (1.4–1.5 eV), one that has not been achieved by any

(12) (a) Jumpertz, E. A. Ueber die Elektronendichteverteilung in der Zinkblende. *Z. Elektrochem.* **1955**, 419. (b) Aminoff G. Untersuchungen ueber die Kristallstrukturen von Wurtzit und Rotnickelkies. *Z. Kristallogr., Kristallgeom., Kristallphys., Kristallchem.* **1923**, 58, 203.

(13) Sato, H.; Mihara, T.; Furuta, A.; Tamura, M.; Mimura, K.; Happo, N.; Taniguchi, M. *Phys. Rev. B* **1997**, 56, 7222.

(14) Parthe, E. Polycrystalline ZnSe (Stilleite, Space Group F43m). *Crystal Chemistry of Tetrahedral Structures*; Gordon and Breach: New York, 1964.

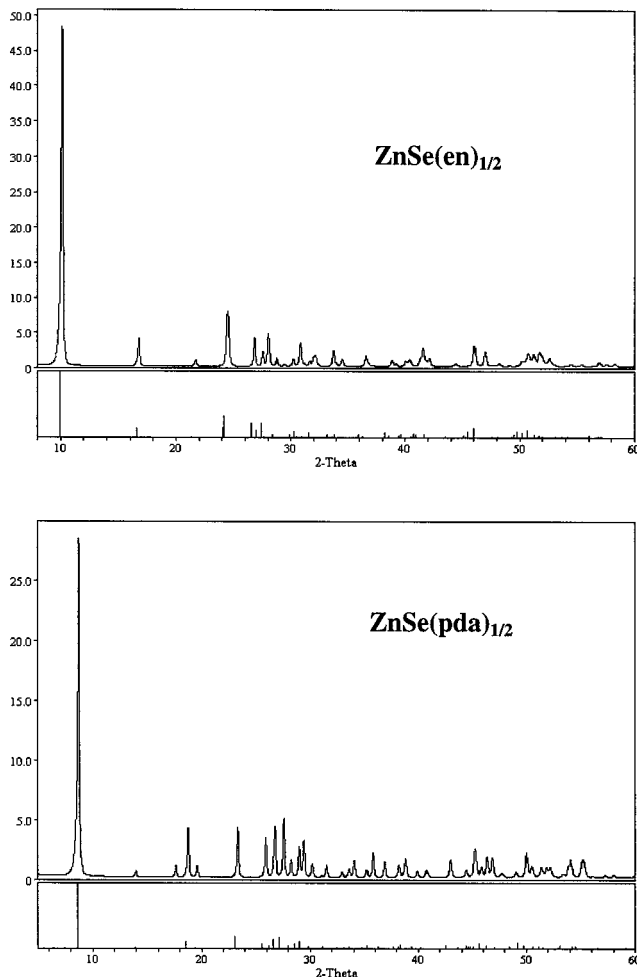


Figure 3. PXRD patterns for [ZnSe(en)_{0.5}] (top) and for [ZnSe(pda)_{0.5}] (bottom). The simulated powder patterns (sticks) from the single-crystal X-ray data of [MnSe(en)_{0.5}] and [MnSe(pda)_{0.5}] are shown as a comparison.

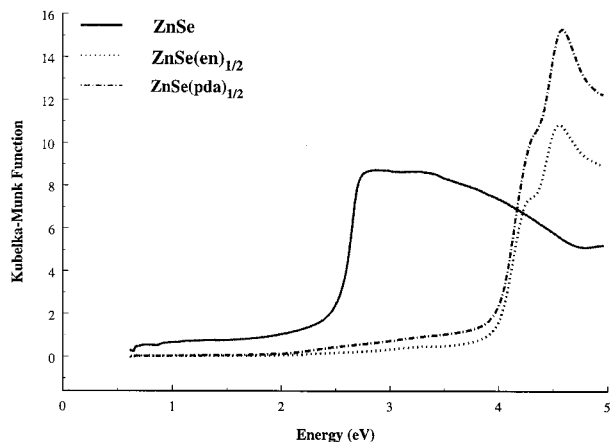


Figure 4. Optical absorption spectra for **3** (dotted line) and **4** (dotted-dashed line), and bulk ZnSe (Stilleite, solid line). The estimated band gap for ZnSe is 2.5 eV, and the on set absorption occurs at 4.0 and 3.9 eV for **3** and **4**, respectively, illustrating a strong blue shift in both cases.

chemically grown colloidal dots. Band structure and transition probability calculations using density functional theory within local density approximation (LDA) have confirmed that the observed large blue shifts in the optical absorption spectra are due to the quantum confinement effect (QCE) of the II–VI layers in these

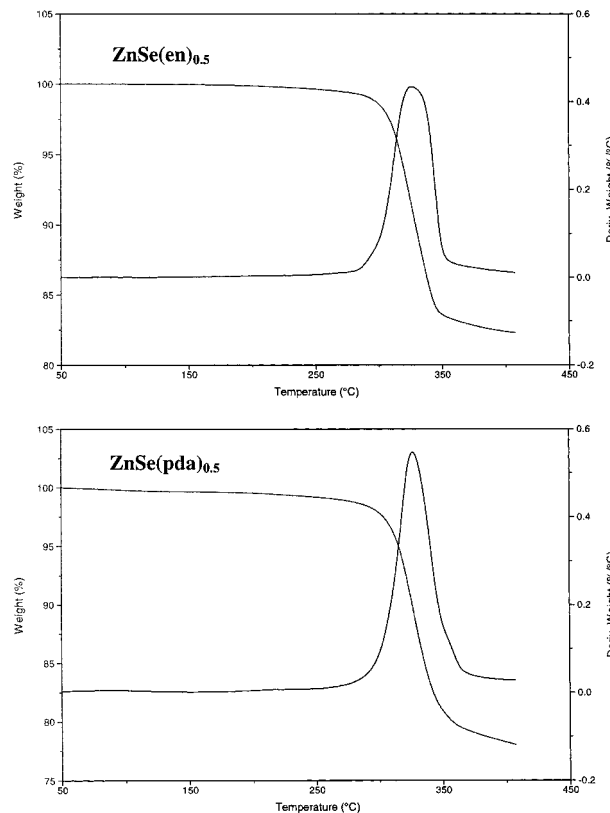


Figure 5. Thermogravimetric analysis data showing weight loss of **3** (top) and **4** (bottom) between 50 and 415 °C. The negative of the first derivative (%/°C) is also plotted as a function of temperature in each case.

hybrid materials.^{5,15} Density of states (DOS) analysis has revealed that II–VI single atomic monolayers contribute extensively to the observed band-edge absorption.

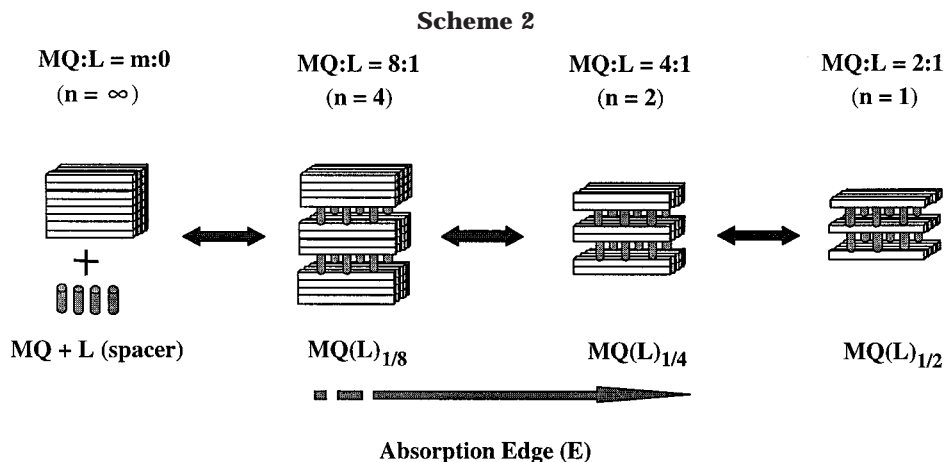
The optical properties of **1** and **2** were also assessed by the same experiments conducted at room temperature. The estimated absorption edges are 1.8 and 1.7 eV for **1** and **2**, respectively, compared to ~1.6 eV measured for the α -MnSe bulk sample (NaCl structure).¹⁶ Note that this value is somewhat smaller than that previously reported E_g for MnSe.¹⁷ While ZnSe-based hybrid compounds (**3**, **4**) exhibit significant changes (1.4–1.5 eV) in their optical absorption edge, it is noted that **1** and **2** give rise to changes in the same direction (increase in energy) with respect to bulk MnSe but to a much smaller extent (0.1–0.2 eV).^{16b} This is due to the fact that the Mn 3d bands are highly localized, and, therefore, the quantum confinement of the $^2_{\infty}$ [MnSe] layers induced by organic spacers via coordinate bonds leads to a much smaller variation in these bands.¹³

Thermal Properties. The TG analyses were performed on polycrystalline samples of **3** and **4**. The weight losses observed for the two compounds, along with the negative values of the first derivatives (%/°C), are shown in Figure 5 as a function of temperature between 50 and 415 °C. Both compounds underwent a

(15) Huang, X.-Y.; Li, J. Unpublished results.

(16) (a) The most stable structure form of MnSe is the NaCl-type structure. See: Baroni, A. Z. *Kristallogr., Kristallgeom., Kristallphys., Kristallchem.* **1938**, *99*, 336. (b) Heulings, H. R.; Huang, X.-Y.; Li, J.; Yuen, T.; Lin, L. L. *Nano Lett.*, in press.

(17) Decker, D. L.; Wild, R. L. *Phys. Rev. B.* **1971**, *4*, 3425.



single-step weight-loss process and were thermally stable up to 250 °C. The measured weight losses of the organic species are 17.7% (2.006 mg) for en (1) and 21.9% (2.270 mg) for pda (2), respectively, in an excellent agreement with the calculated values, 17.3% for en and 20.4% for pda, respectively. The decomposition process completed at approximately 400 °C for both 1 and 2. Powder X-ray diffraction analysis immediately following the TG experiments showed that the residues of both samples contained two isomorphic phases of ZnSe, with the major phase being wurtzite structure ($P6_3mc$) and the minor one, zinc blende structure ($F\bar{4}3m$, Stilleite). The optical diffuse reflectance measurement gave an estimated band gap of ~ 2.7 eV for ZnSe of the wurtzite structure ($P6_3mc$), a small blue shift of 0.2 eV with respect to ZnSe of the zinc blende structure ($F\bar{4}3m$, Stilleite).

Summary

In this work, we have demonstrated that a new type of nanostructures with both strong quantum confinement and periodic arrangement can be synthesized in high yield. Our preliminary studies on other II–VI systems show that they form the same type of hybrids and that strong QCE appears to be a general phenomenon in all these systems.¹⁵ Our approach is unique in that the electrons are confined within the II–VI thin slabs by organic spacers via coordinated bonds, which direct and organize the inorganic slabs into an ordered, crystalline three-dimensional lattice rather than by uncorrelated nanoparticles, as in the case of colloidal dots. Since such confinements are induced internally due to inherent structural properties, they do not depend on the size of the particles. Consequently, the new hybrid nanostructures can be prepared in forms of

micrometer-sized powders via solvothermal routes. Clearly, the uniformity in the structure and the capability in modifying/tuning electronic and optical properties represent the most important features in considering viable candidates for new-generation nanodevices.

Our future study will be mainly on two areas. The first is variation of the slab thickness (n). As illustrated in Scheme 2, the parent II–VI bulk structure (left) and the monolayer hybrid structure (right) represent the two extreme cases where $n = \infty$ and 1, respectively. While the strongest QCE has been achieved at $n = 1$, synthesis of hybrid structures having intermediate n between the two extreme values will allow a controllable tuning of the electronic and optical properties at our demand (see two intermediate cases sketched in Scheme 2, as $n = 2$ and 4). The second area of investigation will involve use of organic spacers (pillars) with variable length and electronic properties. This will enable us to study and to understand the nature of the bonding interactions occurring at the interface of the organic and inorganic components and the effect of such interactions on the structure and properties of the resultant hybrid composites. These efforts shall contribute to our ultimate goal in crystal engineering of new functional materials by design and controlled synthesis.

Acknowledgment. Financial support from the National Science Foundation (Grants DMR-9553066 and DMR-0094872) is greatly appreciated. We thank Dr. H. H. Fu for helpful discussions and comments.

Supporting Information Available: Two X-ray crystallographic files (CIF). This material is available free of charge via the Internet at <http://pubs.acs.org>.

CM010403D